

# D-GAP: Improving Out-of-Domain Robustness via Dataset-Agnostic and Gradient-Guided Augmentation in Frequency and Pixel Spaces

Ruoqi Wang<sup>1</sup>, Haitao Wang<sup>3</sup>, Shaojie Guo<sup>4</sup>, and Qiong Luo<sup>1,2</sup>

<sup>1</sup> HKUST(GZ)

<sup>2</sup> HKUST

<sup>3</sup> SYSU

<sup>4</sup> ECNU

`rwang280@connect.hkust-gz.edu.cn`

**Abstract.** Out-of-domain (OOD) robustness is challenging to achieve in real-world computer vision applications, where shifts in image background, style, and acquisition instruments always degrade model performance. Generic augmentations show inconsistent gains under such shifts, whereas dataset-specific augmentations require expert knowledge and prior analysis. Moreover, prior studies show that neural networks adapt poorly to domain shifts because they exhibit a learning bias to domain-specific frequency components. Perturbing frequency values can mitigate such bias but overlooks pixel-level details, leading to suboptimal performance. To address these problems, we propose **D-GAP**, a **D**ataset-agnostic and **G**radient-guided augmentation method for the **A**mplitude spectrum (in frequency space) and the **P**ixel values, improving OOD robustness by introducing targeted augmentation in both frequency and pixel spaces. Unlike conventional handcrafted augmentations, D-GAP computes sensitivity maps in the frequency space from task gradients, which reflect how strongly the deep models respond to different frequency components, and uses the maps to adaptively interpolate amplitudes between source and target samples. This way, D-GAP reduces the learning bias in frequency space, while a complementary pixel-space blending procedure restores fine spatial details. Extensive experiments on four real-world datasets and three domain-adaptation benchmarks show that D-GAP consistently outperforms both generic and dataset-specific domain adaptation methods, improving average OOD performance by +5.3% on real-world datasets and +1.9% on benchmark datasets.

**Keywords:** Domain adaptation · Data augmentation · OOD robustness

## 1 Introduction

In real-world applications, the distributions in the training datasets often differ from those in other deployment environments because of the shifts in background and acquisition instruments [17, 24]. In such out-of-distribution (OOD) settings,

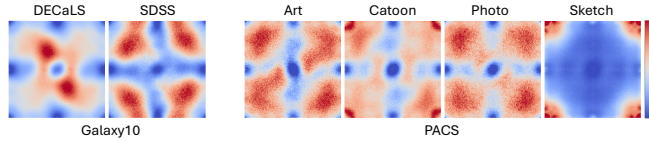


**Fig. 1:** Average Amplitude sensitivity maps of ResNet50 trained on Galaxy10 and PACS datasets across domains.

models trained on source domains always degrade when applied to unlabeled target domains. For example, in wildlife monitoring, ecologists use models to classify species of camera trap images, but these models often show significant accuracy drops when applied to new locations [3]. Annotated data are usually available only for a limited subset of cameras, which may not contain the diversity of environments in the unlabeled target domains. In this paper, we focus on improving OOD robustness in domain adaptation settings, where we have labeled data from source domains and unlabeled data from target domains.

Data augmentation is a common strategy for improving OOD robustness of deep-learning models, but designing effective augmentations remains challenging. Generic augmentations of images (e.g., RandAugment [4], CutMix [45], FACT [41], SAM [40]) improves the performance across datasets to various degrees [9, 12, 38], whereas domain-invariance methods [9, 15, 29, 39, 43, 44, 47] yield limited improvements, especially on real-world domain shifts [8]. Although some dataset-specific augmentation methods [8, 24] can improve OOD performance, they often need expert knowledge and prior analysis of the dataset, which makes these methods hard to scale or apply to new datasets. These limitations highlight the need for more general, dataset-agnostic methods to improve OOD robustness across diverse real-world settings.

Prior studies show that neural networks tend to learn biasedly from different frequency components depending on the dataset’s frequency characteristics [11, 23, 37]. Such spectral bias causes the model to overfit domain-specific frequency components in the frequency spectrum, leading to poor generalization when the target domain has different frequency distributions. As such, we consider that this bias can be reduced by perturbing the data distribution in the frequency space. However, frequency variations mainly reflect texture and style changes, overlooking spatial details. Since the pixel space preserves spatial details and localized pixel-level features which are complementary to frequency information, combining both spaces may address global and local domain shifts simultaneously. Building on this intuition, we propose **D-GAP**, a domain adaptation framework that improves OOD robustness by introducing targeted augmentations in both frequency and pixel spaces. Unlike previous targeted augmentations with manually designed, dataset-specific rules, and work solely in frequency or pixel space, D-GAP automatically adapts to domain shifts from data itself, without the need for expert knowledge or prior analysis.

Specifically, given two images from different domains, in the frequency space, we introduce a gradient-adaptive mechanism in the frequency space that com-

computes frequency sensitivity maps from the task gradients with respect to the amplitude (as shown in Fig. 1). These sensitivity maps represent how strongly the models respond to different frequency components. Instead of interpolating two spectra with a fixed or random ratio, D-GAP adjusts the interpolation strength at each frequency according to its sensitivity value: more sensitive frequency components are more strongly mixed with target-domain amplitudes, while less sensitive ones are more preserved. This mechanism enables the models to suppress domain-specific spectral learning bias by perturbing biased with varying intensities. This gradient-guided interpolation creates frequency-space augmentations that adaptively keep the main content of the source image while adding features from target domains. However, frequency blending and reconstruction sometimes introduce artifacts and blurring. As such, we apply pixel value blending to add complementary spatial pixel-level information. The final augmented image is then obtained by blending these two results from the frequency space and the pixel space.

We evaluate our method on four real-world datasets: wildlife recognition (iWildCam [2, 25]), tumor detection (Camelyon17 [1, 25]), bird species recognition (BirdCalls [8, 16]), and galaxy morphology classification (Galaxy10 DECaLS & SDSS [13]). Extensive experiments demonstrate that D-GAP consistently outperforms other baselines. Compared to other generic methods, D-GAP achieves improvements in OOD performance, including +2.1% gains on iWildCam, +4.2% on Camelyon17, +5.6% on BirdCalls, and +9.3% on Galaxy10. Also, our method surpasses dataset-specific augmentation strategies tailored for different datasets. Additionally, D-GAP also makes average gains of +1.9% accuracy on standard benchmark datasets (PACS [19], Office-Home [34], and Digits-DG [47]), showing its improvement across diverse distribution shifts. We further analyze the generalizability of D-GAP on various backbone networks and the its effectiveness of connecting same-class cross-domain samples while separating different-class examples.

Our work makes the following contributions: (1) We propose D-GAP, a dataset-agnostic target augmentation method that works in both the frequency and pixel spaces, through gradient-guided amplitude interpolation and spatial blending, respectively. (2) Our method is general and adaptive, with strong performance in real-world applications without dataset-specific manipulation. (3) We achieve state-of-the-art results across multiple backbones on both real-world and general benchmark datasets.

## 2 Background and Formulation

### 2.1 Feature Decomposition

To better understand how models perform under domain shifts, we use the feature decomposition framework [8], which categorizes input features based on their dependence on the label and domain. Specifically, input features can be decomposed into four types based on their dependence on the label and the domain: (1) features that are *label-dependent* and *domain-independent* ( $x_{obj}$ ); (2)

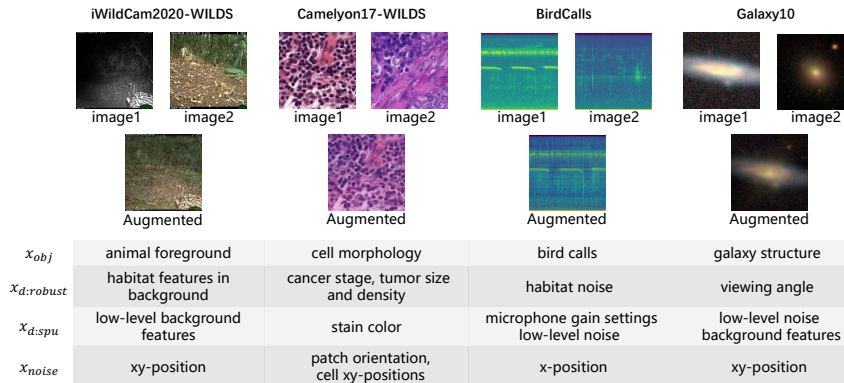


**Fig. 2: Feature decomposition and augmentation examples.** *Top:* For each dataset (iWildCam, Camelyon17, BirdCalls, Galaxy10), we show a source image, its corresponding augmented image generated by our method. *Bottom:* Based on the decomposition framework [28], we annotate representative features in the datasets across  $x_{obj}$ ,  $x_{d:robust}$ ,  $x_{d:spu}$ ,  $x_{noise}$ . Our method effectively randomizes  $x_{d:spu}$ , varies  $x_{d:robust}$  while preserving or  $x_{obj}$ .

*label-dependent* and *domain-dependent* features ( $x_{d:robust}$ ); (3) *label-independent* and *domain-dependent* features ( $x_{d:spu}$ ); and (4) *label-independent* and *domain-independent* features ( $x_{noise}$ ). We formalize these relationships via their dependence with the label  $y$  and domain  $d$ :

$$x_{obj}, x_{d:robust} \not\perp y, \quad x_{noise}, x_{d:spu} \perp\!\!\!\perp y,$$

$$x_{d:robust}, x_{d:spu} \not\perp d, \quad x_{obj}, x_{noise} \perp\!\!\!\perp d.$$

Models should focus on both  $x_{obj}$  and  $x_{d:robust}$  while avoiding reliance on spurious or noisy features [8]. We later analyse these relationships using a connectivity-based framework (Section 2.4 and 4.5) to evaluate how augmentations influence these label/domain dependent features.

## 2.2 Datasets

**Real-World Datasets.** As shown in Fig. 2, we test our method on four real-world datasets in this paper: **iWildCam** [2, 17] – wildlife species classification with location-related background shifts. **Camelyon17** [1, 17] – tumor identification across hospitals with stain and density variations. **BirdCalls** [8, 16] – bird species recognition under habitat and microphone domain noise. **Galaxy10** [13] – galaxy morphology classification across telescopes differing in resolution and color profile. Each dataset presents distinct domain shifts such as environmental background, staining style, recording device, or instrument differences. More dataset details are provided in Appendix Section B.

**Additional Benchmark Datasets.** In addition to the four real-world datasets used throughout this paper, we further evaluate our method on three standard benchmarks: **PACS** [19], **Office-Home** [34], and **Digits-DG** [47]. Compared to our four real-world datasets that cover diverse real-world scenario and deployment-related shifts, these benchmarks datasets focus on visual recognition with well-studied style variations. More details provided in Appendix Section B.

### 2.3 Targeted Augmentations

Some dataset-specific augmentation methods [8, 24] can improve OOD performance on real-world applications. However, they often need expert knowledge and prior analysis of the dataset, which makes these methods hard to scale or apply to new datasets. For instance, in wildlife recognition, some methods randomize the background of camera trap images to mitigate spurious correlations between results and location-specific terrains or lighting conditions. Such a target augmentation helps the model to focus on the animal foreground. However, it depends on the segmentation of foreground and background, restricting its application to datasets without foreground annotations. Similarly, in tumor identification from histopathology slides, Stain Color Jitter can deal with stain color variations across hospitals [33]. It perturbs images within the hematoxylin and eosin staining features to overcome color-related domain biases, while preserving morphological features [8]. However, it requires expert knowledge of staining chemistry and color editing. These examples show that while dataset-specific augmentations can be effective, they are difficult to generalize.

### 2.4 Connectivity

To better understand how data augmentations impact cross-domain generalization, we adopt the concept of *connectivity* [28]. We define connectivity between a class-domain pair  $((y_1, d_1), (y_2, d_2))$  under four conditions:

$$\left\{ \begin{array}{ll} \rho : y_1 = y_2, d_1 = d_2. & \text{(same class, same domain)} \\ \alpha : y_1 = y_2, d_1 \neq d_2. & \text{(same class, different domains)} \\ \beta : y_1 \neq y_2, d_1 = d_2. & \text{(different classes, same domain)} \\ \gamma : y_1 \neq y_2, d_1 \neq d_2. & \text{(different classes, different domains)} \end{array} \right. \quad (1)$$

Here, each of the  $\rho, \alpha, \beta, \gamma$  values indicates how “connected” a pair is. Shen et al. [28] show that the ratios  $\frac{\alpha}{\gamma}$  and  $\frac{\beta}{\gamma}$  exhibit strong empirical correlation with OOD accuracy. In this work, we follow this approach to show how our augmentation changes the connectivity of the data. More details on the computation of connectivity are presented in Section 4.5 and the Appendix Section D. To improve OOD robustness, the model must randomize features that depend on specific domains while preserving task-relevant information. Specifically, in feature decomposition [28], we randomize domain-dependent features ( $x_{d:\text{spu}}$ ) and keep label-relevant ones ( $x_{\text{obj}}, x_{d:\text{robust}}$ ). As shown in Fig. 3, we observe that

amplitude mixing in frequency domain (Details of the mixing strategy are provided in Section 3.) preserves task-relevant semantic structure [41] ( $x_{\text{obj}}$  and  $x_{d:\text{robust}}$ ), while effectively randomizing  $x_{d:\text{spu}}$ . However, solely frequency mixing may introduce artifacts and blurring (as examples in Fig. 3 and 4), influencing the extraction of detailed features.

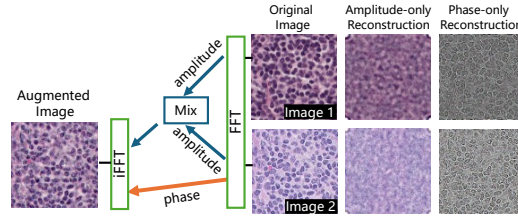


**Fig. 3:** The figure shows the amplitude-only and phase-only reconstructions of the two input images, and the process where the amplitudes of Image 1 and Image 2 are first mixed, and the mixed amplitude is combined with the phase of Image 2 to generate an augmentation of Image 2.

**Table 1:** Comparison of connectivity values and ratio on iWildCam dataset.

| Datasets  | $\alpha$ | $\beta$ | $\gamma$ | $\alpha/\gamma$ | $\beta/\gamma$ |
|-----------|----------|---------|----------|-----------------|----------------|
| Original  | 0.007    | 0.008   | 0.021    | 0.33            | 0.38           |
| Augmented | 0.212    | 0.030   | 0.051    | 4.16            | 0.59           |

To address the problem, we add pixel-space mixing as a complement, which brings back more pixel-level details and perturbs  $x_{d:\text{spu}}$ . However, it may influence  $x_{\text{obj}}$  and  $x_{d:\text{robust}}$  as well. Therefore, we then define a tunable ratio (details are in Section 3). By combining the augmentation in both frequency and pixel spaces, our goal is to balance the label-relevant and domain-relevant shifts, achieving domain diversity while maintaining semantic identity. This dual-space augmentation enables fine-grained control over domain perturbation intensity and promotes robust feature learning across source and unseen domains. We then empirically evaluate our method by comparing the connectivity ratios  $\frac{\alpha}{\gamma}$  and  $\frac{\beta}{\gamma}$  of the augmented and unaugmented datasets. Results in Table 1 show that augmentation in frequency-pixel spaces can enhance the cross-domain connectivity, achieving domain diversity while maintaining label-relevant identity.

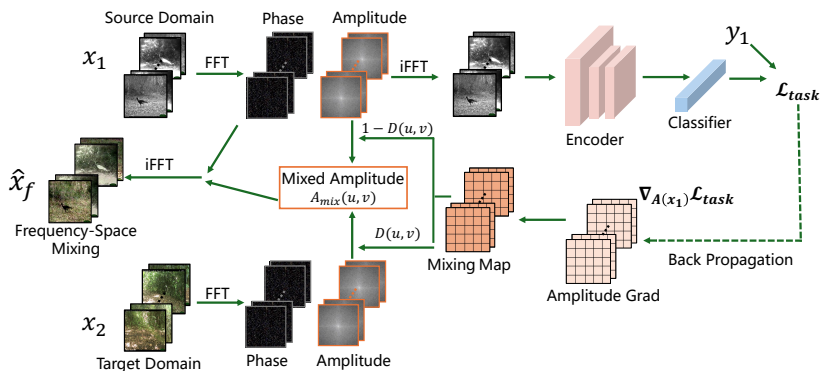


**Fig. 4:** Overview of the Gradient-guided Amplitude Mix procedure. Given a source image  $x_1$  and a target-domain image  $x_2$ , we compute the Sensitivity Map  $G(u, v)$  and the Mixing Map  $D(u, v)$ . The mixed amplitude is then combined with the phase of  $x_1$ .

### 3 Method

In this section, we introduce the technical details of D-GAP, including Fourier transform preliminaries and details of each module, including the Gradient-guided Amplitude Mix, Pixel-Space Mixing, and the training framework.

#### 3.1 D-GAP

**Fourier Transform of Images.** For an image  $x$ , its Fourier transformation  $\mathcal{F}(x)$  is formulated as:

$$\mathcal{F}(x)(u, v) = \sum_{h=0}^{H-1} \sum_{w=0}^{W-1} x(h, w) e^{-j2\pi(\frac{hu}{H} + \frac{wv}{W})}, \quad (2)$$

where  $(u, v)$  are coordinates in the frequency space.  $\mathcal{F}^{-1}(x)$  denotes the corresponding inverse Fourier transformation. Both forward and inverse Fourier transforms can be efficiently computed via the Fast Fourier Transform (FFT) algorithm.

The amplitude and phase components of  $\mathcal{F}(x)$  are computed respectively as:

$$\begin{aligned} \mathcal{A}(x)(u, v) &= [R^2(x)(u, v) + I^2(x)(u, v)]^{1/2}, \\ \mathcal{P}(x)(u, v) &= \arctan\left(\frac{I(x)(u, v)}{R(x)(u, v)}\right). \end{aligned} \quad (3)$$

where  $R(x)$  and  $I(x)$  denote the real and imaginary parts of  $\mathcal{F}(x)$ , respectively. For RGB images, the Fourier transform is applied to each channel separately.

**Gradient-guided Amplitude Mix.** Conventional frequency-based augmentations [40, 41] typically mix amplitudes of two images with a random intensity factor. While such random interpolation introduces diversity, it fails to

distinguish how sensitive that the model is to each frequency component. Moreover, the interpolation ratio need to be manually constrained within a predefined range to avoid excessive distortion. To overcome these limitations, D-GAP performs a gradient-guided amplitude mix, adaptively adjusting the interpolation strength based on the model’s sensitivity in the frequency space. The process of Gradient-guided Amplitude Mix is shown in Fig. 4.

Given two source images  $x_1$  and  $x_2$ , we aim to augment  $x_1$  by injecting the amplitude information of  $x_2$  into a square region  $\Omega_r$  in the Fourier space. Let  $f$  denote the classifier and  $\mathcal{L}_{\text{task}}$  the supervised loss. We compute the gradient of the loss with respect to the source amplitude:

$$G(u, v) = \left| \frac{\partial \mathcal{L}_{\text{task}}(f(x_1), y)}{\partial A(x_1)(u, v)} \right|, \quad (u, v) \in \Omega_r. \quad (4)$$

Here,  $G(u, v)$  measures the model’s sensitivity to each frequency, which means how much the task loss would change if the amplitude at a specific frequency  $(u, v)$  were perturbed. In this paper, we call  $G(u, v)$  as **sensitivity map**. Large gradient values indicate that the model’s prediction heavily depends on that frequency component, implying stronger spectral bias. This allows D-GAP to continuously regulate how much information to mix at each frequency.

Then after normalizing  $G$  and applying a sigmoid function,

$$\tilde{G} = \frac{G - \mu(G)}{\sigma(G) + \varepsilon}, \quad D = \text{clip}(\text{Sigmoid}(\tilde{G}), d_{\min}, d_{\max}), \quad (5)$$

we obtain a gradient-based **mixing map**  $D(u, v)$  from the sensitivity map  $G(u, v)$  that adaptively controls the amplitude interpolation. In our design, higher sensitivity (larger  $G(u, v)$ ) leads to stronger interpolation from the target domain, encouraging the model to replace its frequency-biased components with cross-domain information. Conversely, D-GAP uses weaker interpolation in lower sensitivity regions to preserve non-biased features. The final adaptive interpolation is computed as:

$$A_{\text{mix}}(u, v) = (1 - D(u, v)) A(x_1)(u, v) + D(u, v) A(x_2)(u, v), \quad (u, v) \in \Omega_r. \quad (6)$$

Finally, the mixed image is reconstructed as

$$\begin{aligned} \mathcal{F}_{\text{mix}}(u, v) &= A_{\text{mix}}(u, v) e^{-jP(x_1)(u, v)}, \\ \hat{x}_f &= \mathcal{F}^{-1}(\mathcal{F}_{\text{mix}}). \end{aligned} \quad (7)$$

Through this gradient-guided strategy, D-GAP adaptively perturbs spectral values with target domain more strongly where the model exhibits higher frequency bias. This data-driven, continuous modulation mitigates models’ reliance on domain-specific spectral shortcuts, encouraging the model to learn more balanced and generalizable representations across domains.

**Pixel-Space Mixing:** Frequency blending sometimes introduces artifacts and blurring in the resulting augmentations. As a result, in addition to frequency-domain augmentation, we introduce a pixel-space mixing strategy to add more pixel-level details in the augmentation. Specifically, given a source image  $x$  and a target image  $x'$ , we apply pixel-wise blending with ratio  $\lambda_1$ :

$$\hat{x}_p = (1 - \lambda_1)x_1 + \lambda_1x_2, \quad (8)$$

Then, we combine both pixel-space and frequency-space augmented images via a second-stage blending:

$$\hat{x} = (1 - \lambda_2)\hat{x}_f + \lambda_2\hat{x}_p, \quad (9)$$

This two-stage fusion allows us to perturb frequency bias while maintaining the semantic content of the original sample and the pixel details.

### 3.2 Training Framework

Our training strategy follows established practices in prior works [18, 24, 40, 41].

**Real-world datasets.** For real-world datasets (e.g., *iWildCam*, *Camelyon17*, *BirdCalls*, and *Galaxy10*), we use the **Linear Probing then Fine-Tuning (LP-FT)** strategy [18, 24]. We first train a linear classifier on frozen pretrained features to stabilize early optimization, then fine-tune both the encoder and classifier using D-GAP augmentations. This procedure improves OOD robustness by gradually adapting high-level representations to domain-diverse augmentations while preventing early-stage overfitting.

**Common DG Benchmarks.** For domain generalization benchmarks (i.e., *PACS*, *Office-Home*, *Digits-DG*), we follow previous works [40, 41] to train directly on the pretrained encoder without the LP-FT stage for fair comparisons. On these datasets, the pretrained model already provides a stable initialization, and applying D-GAP augmentations directly during training yields efficient adaptation and robust convergence.

## 4 Experiments

In this section, we first conduct comparisons between D-GAP and other recent methods on various datasets. We also conduct an ablation study to evaluate the contribution of each module in D-GAP. We then evaluate how our method generalizes beyond backbone networks. Finally, we conduct a connectivity analysis on empirical evidence of how our dual-space augmentation enhances cross-domain feature alignment.

### 4.1 Experimental Settings

**Platform:** We conduct the experiments on a server with 128 AMD EPYC 7543 32-Core Processors, 512GB main memory, and eight NVIDIA RTX A6000 GPUs,

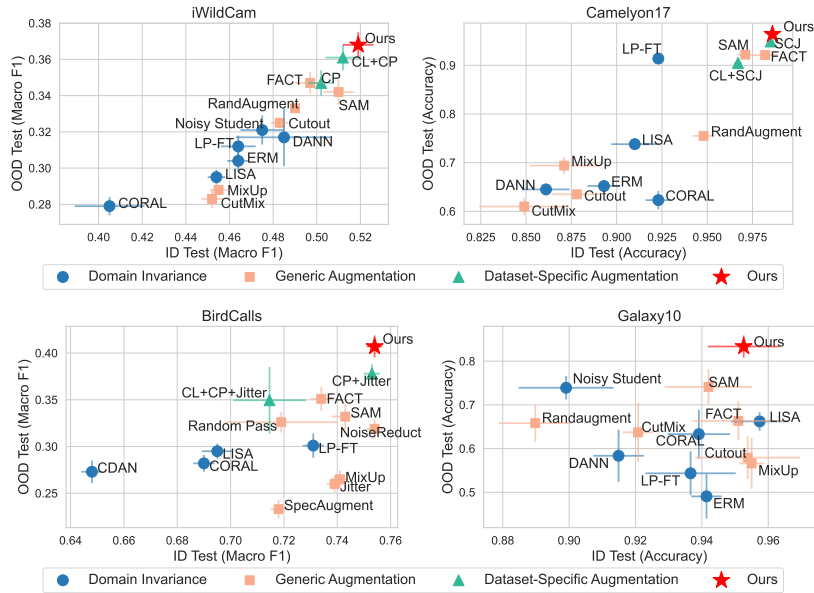


**Fig. 5:** We plot the in-domain (ID) performance versus out-of-domain (OOD) performance for all methods across four datasets. Our method consistently outperforms all baselines in OOD generalization. ‘CL’ refers to ‘Connect Later’. ‘CP’ refers to ‘Copy Paste’. ‘SCJ’ refers to ‘Stain Color Jitter’.

each with 48GB device memory. The operating system is Ubuntu 22.04. Our model is implemented in PyTorch 2.1.0.

**Evaluation Metrics:** Following previous work [8, 24, 27, 35, 40, 41], we select metrics that best suit the characteristics of each dataset to ensure a comprehensive evaluation of model performance. We use F1 score and accuracy as evaluation metrics, depending on the nature of the task and dataset. The F1 score is used for iWildCam, BirdCalls datasets to account for class imbalance, and we use accuracy for Camelyon17, Galaxy10, PACS, Digits-DG and OfficeHome.

**Method under Comparison:** We compare our method against various baseline approaches for domain generalization and out-of-domain (OOD) performance enhancement. These baselines include: **(1) Generic Augmentations and Domain Invariance Baselines.** For real-world dataset iWildCam, Camelyon17 and Galaxy10, we compare our approach with several commonly used augmentation techniques: RandAugment [4], CutMix [45], MixUp [46], Cutout [5], FACT [41], and SAM [40]. In the case of the BirdCalls dataset, we compare with MixUp, SpecAugment [22], random low/high pass filters, noise reduction [26], Jitter [8, 33], FACT [41], and SAM [40]. We also compare to LISA [44], a method designed to encourage domain invariance by applying mixing augmentations to inputs of the same class across different domains. Additionally, we evaluate other domain invariance algorithms that do not rely on augmentation,

including DANN [7, 21], DeepCORAL [30, 31], and ERM [24], LP-FT [18]. For the DG benchmark datasets, we compared with four state-of-the-art baselines FACT [41], SAM [40], Su et al, [29] (following the setting of DA + DeepCoral), and AGST [39]. **(2) Dataset-Specific Targeted Augmentations.** We also compare our method with dataset-specific targeted augmentations [8] for real-world datasets: Copy-Paste for iWildCam, Stain Color Jitter for Camelyon17, and Copy-Paste + Jitter for BirdCalls. We also compare to the latest SOTA method Connect Later, which includes the dataset-specific targeted augmentations in the finetuning procedure after pretraining [24].

**Backbone Networks:** In section 4.2, 4.3, we use the same pretrained backbones as [8, 24] for iWildCam (ResNet50 [10]), Camelyon17 (DenseNet-121 [14]) and BirdCalls (EfficientNet-B0 [32]). For Galaxy10, we follow [36] to use ResNet18 [10] for better performance. And we use the same ConvNet backbone as [40, 41, 47, 48] for Digits-DG, and ResNet18 [10] for OfficeHome and PACS. Details are presented in the Appendix Section C. We also additionally evaluate our method in 4.4 with ViT [6] and ConvNeXt [20] backbone networks to verify that D-GAP generalizes beyond backbone choices.

## 4.2 Comparison Results

Fig. 5 summarizes the in-domain (ID) and out-of-domain (OOD) performance for all methods across four real-world datasets: iWildCam, Camelyon17, BirdCalls, and Galaxy10. Each point represents one method, colors and shapes represent method types, and our method is marked as a red star.

**Results on Real-World Datasets.** Our method consistently achieves the best OOD performance across all four real-world datasets, while maintaining a strong ID performance. Notably, our approach significantly outperforms all generic methods, including **generic augmentation** and **domain invariance** baselines that do not require dataset-specific design or prior knowledge. Compared to the best generic method (FACT) on iWildCam, our method improves OOD Macro F1 from 34.7% to 36.8%. On Camelyon17, our approach achieves 96.4% OOD accuracy, outperforming the best generic augmentation (SAM at 92.2%) and the best domain invariance method (LP-FT at 91.4%). On BirdCall, OOD Macro F1 increases from 35.1% (FACT) to 40.7%, and on Galaxy10, our method improves OOD accuracy from 74.1% (SAM) to 83.4%.

Moreover, our method also outperforms **dataset-specific augmentation** methods Connect Later + Copy-Paste on iWildCam, Connect Later + Stain Color Jitter on Camelyon17, and Connect Later + Copy-Paste + Jitter on BirdCalls, all of which require expert knowledge and manual design tailored for the dataset based on its characteristics. In contrast, our method is in a fully **dataset-agnostic** way, but still achieves superior or comparable results. These results show that our method is not only effective but also broadly applicable, without relying on dataset-specific analysis or prior knowledge.

**Results on Common Benchmarks.** Tables 2, 3 and 4 summarize the leave-one-domain-out results on PACS, Digits-DG, and Office-Home. The results of FACT and SAM in these tables are copied from the source paper [40] for fair

comparison, as our re-implementations under identical settings produced slightly lower numbers. In these tables, DeepAll refers to vanilla backbones trained from a simple aggregation of all source data [42]. Our method achieves the highest average accuracy on all three benchmarks (PACS: **89.03**, Digits-DG: **84.5**, Office-Home: **70.22**). These results show that the proposed dual-space targeted augmentation is dataset-agnostic and robust to different domain variations, while our focus remains on real-world deployment/environment shifts.

### 4.3 Ablation Study

Table 5 presents ablation results of the effects of pixel-space and frequency-space mixing, as well as the impact of the gradient-guided mechanism. Across the four real-world datasets, our full method achieves the highest OOD performance, outperforming LP-FT [18] and all single-modality or an unguided variant (replacing the mixing map with unified mixing ratio in frequency space, denoted Ours\_v1). We also tested fixed mixing masks in frequency domain and mix the masked region with the target using a constant ratio, and compared three choices *low-frequency mask*, *high-frequency mask*, and *ring mask*.

Frequency-only mixing consistently outperforms pixel-only mixing—especially on Camelyon17 and Galaxy10—highlighting the importance of frequency-space perturbation. Replacing the gradient-guided mechanism (w/o grad-guide) leads to a consistent drop in OOD performance, confirming that this adaptive, sensitivity-aware guidance is essential for robust domain adaptation.

### 4.4 Generalization on Backbone Networks

To verify that D-GAP generalizes beyond backbone networks, we additionally evaluate with **ConvNeXt-Tiny** [20] and **ViT-B/16** [6]. Table 6 shows that D-GAP consistently improves OOD performance on PACS, Digits-DG, and OfficeHome under both backbones. Fig. 6 further visualizes the ID–OOD trade-off on Galaxy10, where D-GAP remains SOTA performance on OOD robustness.

### 4.5 Empirical Evaluations of Connectivity

To better understand why our method is effective on improving OOD robustness, we take iWildCam and Camelyon17 as examples and empirically evaluate

**Table 2:** Model accuracy of leave-one-domain-out evaluation on PACS. The best and second-best results are bold and underlined, respectively.

| Methods               | Art          | Cartoon      | Photo        | Sketch       | Avg.         |
|-----------------------|--------------|--------------|--------------|--------------|--------------|
| DeepAll               | 84.94        | 76.98        | <u>97.64</u> | 76.75        | 84.08        |
| FACT (2023) [41]      | <b>89.68</b> | 81.06        | 97.02        | 83.76        | <u>87.88</u> |
| SAM (2023) [40]       | 85.25        | <u>82.02</u> | 96.75        | <u>85.04</u> | 87.27        |
| Su et al. (2024) [29] | 79.88        | 78.03        | 95.93        | 73.15        | 81.75        |
| AGST (2025) [39]      | 83.50        | 80.83        | 96.49        | 79.57        | 85.35        |
| <b>Ours</b>           | <u>89.34</u> | <b>82.81</b> | <b>97.99</b> | <b>85.98</b> | <b>89.03</b> |

**Table 3:** Model accuracy of leave-one-domain-out evaluation on Digits-DG. The best and second-best results are bolded and underlined, respectively.

| Methods               | MNIST       | MNIST-M     | SVHN        | SYN         | Avg.        |
|-----------------------|-------------|-------------|-------------|-------------|-------------|
| DeepAll               | 95.8        | 58.8        | 61.7        | 78.6        | 73.7        |
| FACT (2023) [41]      | <u>97.9</u> | 65.6        | 72.4        | 90.3        | 81.5        |
| SAM (2023) [40]       | 97.8        | <u>66.8</u> | 73.2        | 90.7        | 82.1        |
| Su et al. (2024) [29] | 97.3        | 65.9        | <u>74.5</u> | 92.5        | <u>82.6</u> |
| AGST (2025) [39]      | 97.3        | 63.1        | <u>70.2</u> | 93.2        | 81.0        |
| <b>Ours</b>           | <b>98.3</b> | <b>68.5</b> | <b>77.2</b> | <b>93.8</b> | <b>84.5</b> |

**Table 4:** Model accuracy of leave-one-domain-out evaluation on OfficeHome. The best and second-best results are bolded and underlined, respectively.

| Methods               | Art          | Clipart      | Product      | Real         | Avg.         |
|-----------------------|--------------|--------------|--------------|--------------|--------------|
| DeepAll               | 57.88        | 52.72        | 73.50        | 74.80        | 64.72        |
| FACT (2023) [41]      | 60.34        | 54.85        | 74.48        | <u>76.55</u> | 66.56        |
| SAM (2023) [40]       | 60.79        | <b>55.47</b> | 74.37        | <u>76.37</u> | 66.75        |
| Su et al. (2024) [29] | 64.13        | 54.83        | <u>75.60</u> | 75.36        | <u>67.71</u> |
| AGST (2025) [39]      | 62.50        | 53.87        | <u>74.57</u> | 75.70        | 66.66        |
| <b>Ours</b>           | <b>64.82</b> | <u>55.21</u> | <b>77.76</b> | <b>83.08</b> | <b>70.22</b> |

the connectivity measures. The process of computing the average connectivity between two class-domain pairs  $(c, d)$  and  $(c', d')$  involves labeling all training examples from class  $c$  and domain  $d$  as 0, and those from class  $c'$  and domain  $d'$  as 1, while discarding examples from other classes or domains. Then, we train a ResNet50 [10] model (Training details are presented in Appendix). The test set is prepared similarly to the training set, and the model’s performance on the test dataset provides an estimate of connectivity between the specified class-domain pairs, quantified by the test error rate. Specifically, we train binary classifiers from scratch to predict the class-domain pair of each input example. For iWild-Cam, we randomly select 15 class-domain pairs, while for Camelyon17, we use all class-domain pairs since it is a binary classification task. We use Ours\_v1 for connectivity estimation to exclude the effect of gradient-adaptive modulation and focus on how dual-space mixing influences cross-domain feature connectivity.

**Table 5:** Ablation results across four real-world datasets.

|                | iWildCam (F1) |             | Camelyon17 (Acc) |             | BirdCall (F1) |             | Galaxy10 (Acc) |             |
|----------------|---------------|-------------|------------------|-------------|---------------|-------------|----------------|-------------|
|                | ID            | OOD         | ID               | OOD         | ID            | OOD         | ID             | OOD         |
| LP-FT          | 46.4          | 31.2        | 92.3             | 91.4        | 73.1          | 30.1        | 93.6           | 54.3        |
| Pixel-only     | 45.4          | 29.1        | 87.5             | 69.8        | 75.2          | 32.4        | 95.5           | 68.2        |
| Frequency-only | <b>52.0</b>   | 35.6        | 98.3             | 95.7        | 73.4          | 37.6        | 95.1           | 77.9        |
| Mask-low       | 51.2          | 36.0        | 98.3             | 96.1        | 75.5          | 38.4        | 95.1           | 80.5        |
| Mask-high      | 51.5          | 35.4        | 97.9             | 95.4        | 75.1          | 36.4        | 95.0           | 79.5        |
| Mask-ring      | 51.9          | 34.3        | 98.2             | 94.0        | 74.9          | 36.5        | <b>95.7</b>    | 77.1        |
| Ours_v1        | <u>51.3</u>   | <u>36.3</u> | <b>98.7</b>      | <u>96.3</u> | <b>75.7</b>   | <u>38.3</u> | <b>95.7</b>    | 80.8        |
| <b>Ours</b>    | <u>51.9</u>   | <b>36.8</b> | <u>98.6</u>      | <b>96.4</b> | <u>75.4</u>   | <b>40.7</b> | 95.3           | <b>83.4</b> |

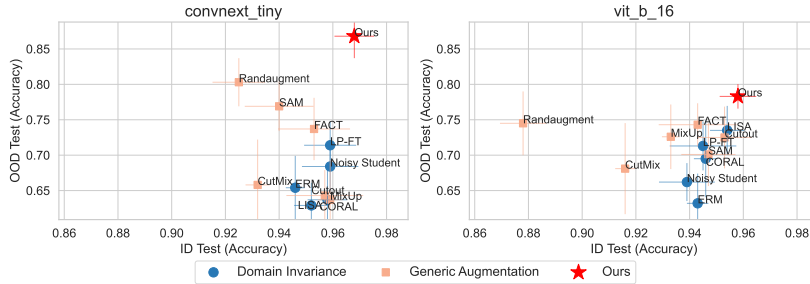


**Fig. 6:** Performance of ConvNeXt and ViT on Galaxy10.

**Table 6:** Average performance on PACS, Digits-DG, and OfficeHome with ConvNeXt and ViT backbones.

| Method                | PACS        |             | Digits      |             | OfficeHome  |             |
|-----------------------|-------------|-------------|-------------|-------------|-------------|-------------|
|                       | ConvNeXt    | ViT         | ConvNeXt    | ViT         | ConvNeXt    | ViT         |
| SAM (2023) [40]       | 85.3        | 85.4        | 88.0        | 85.1        | 73.7        | 63.8        |
| Su et al. (2024) [29] | 87.9        | 75.3        | 88.9        | 85.6        | 73.9        | 64.6        |
| AGST (2025) [39]      | 87.4        | 79.0        | 88.5        | 85.8        | 73.7        | 64.4        |
| Ours                  | <b>88.7</b> | <b>86.4</b> | <b>89.8</b> | <b>86.8</b> | <b>75.0</b> | <b>66.0</b> |

We present connectivity ratios  $\alpha/\gamma$  and  $\beta/\gamma$  on datasets Camelyon17 and iWildCam in Table 7. As shown in Table 7, our method achieves the highest  $\alpha/\gamma$  value on both datasets, showing more consistent semantic alignment across domains as well as more effective randomization of spurious domain-dependent features  $x_{d:\text{spu}}$ . However, a moderate  $\beta/\gamma$  indicates our method may also slightly perturbs class-relevant features  $x_{\text{obj}}, x_{d:\text{robust}}$ . However, from Table 5 and Fig. 5, our method still achieves the best OOD performance. This result is consistent with the estimation proposed by Shen et al. [28], where the target accuracy is estimated to be  $(\alpha/\gamma)^{w_1} \cdot (\beta/\gamma)^{w_2}$ , with higher weight on  $\alpha/\gamma$  (i.e.,  $w_1 > w_2$ ). These results show that our method achieves a balance of preservation of class-relevant features and perturbation of domain-relevant features.

## 5 Conclusion, Limitations and Future Work

We propose D-GAP, providing a simple and adaptive approach for OOD robustness without dataset-specific analysis. By operating in both frequency and pixel spaces and adaptively interpolating amplitude values, our method achieves notable improvements on multiple real-world datasets and common domain adaptation datasets.

One limitation is that the current framework needs additional gradient computation in every training batch during augmentation, which takes extra training time. In future work, we aim to improve the efficiency of our gradient-adaptive augmentation mechanism. Moreover, integrating our augmentation scheme with

**Table 7:** Comparison of connectivity across class, domain, and both for different methods on Camelyon17 and iWildCam datasets.

| Dataset    | Augmentations      | $\alpha$ | $\beta$ | $\gamma$ | $\alpha/\gamma$ | $\beta/\gamma$ |
|------------|--------------------|----------|---------|----------|-----------------|----------------|
| Camelyon17 | w/o Augmentations  | 0.015    | 0.189   | 0.002    | 7.50            | 94.5           |
|            | RandAugment        | 0.181    | 0.186   | 0.114    | 1.59            | 1.63           |
|            | Stain Color Jitter | 0.029    | 0.116   | 0.004    | 7.25            | 29.0           |
|            | Ours_v1            | 0.120    | 0.073   | 0.003    | 40.0            | 24.3           |
| iWildCam   | w/o Augmentations  | 0.007    | 0.008   | 0.021    | 0.33            | 0.38           |
|            | RandAugment        | 0.224    | 0.125   | 0.130    | 1.72            | 0.96           |
|            | Copy-Paste         | 0.254    | 0.031   | 0.063    | 4.03            | 0.49           |
|            | Ours_v1            | 0.212    | 0.030   | 0.051    | 4.16            | 0.59           |

foundation models or self-supervised objectives may further improve OOD robustness in label-scarce or zero-shot settings.

## References

- Bandi, P., Geessink, O., Manson, Q., Van Dijk, M., Balkenhol, M., Hermsen, M., Bejnordi, B.E., Lee, B., Paeng, K., Zhong, A., et al.: From detection of individual metastases to classification of lymph node status at the patient level: the camelyon17 challenge. *IEEE transactions on medical imaging* **38**(2), 550–560 (2018)
- Beery, S., Agarwal, A., Cole, E., Birodkar, V.: The iwildcam 2021 competition dataset. *arXiv preprint arXiv:2105.03494* (2021)
- Beery, S., Van Horn, G., Perona, P.: Recognition in terra incognita. In: *Proceedings of the European conference on computer vision (ECCV)*. pp. 456–473 (2018)
- Cubuk, E.D., Zoph, B., Shlens, J., Le, Q.V.: Randaugment: Practical automated data augmentation with a reduced search space. In: *Proceedings of the IEEE/CVF conference on computer vision and pattern recognition workshops*. pp. 702–703 (2020)
- DeVries, T., Taylor, G.W.: Improved regularization of convolutional neural networks with cutout. *arXiv preprint arXiv:1708.04552* (2017)
- Dosovitskiy, A., Beyer, L., Kolesnikov, A., Weissenborn, D., Zhai, X., Unterthiner, T., Dehghani, M., Minderer, M., Heigold, G., Gelly, S., et al.: An image is worth 16x16 words: Transformers for image recognition at scale. *arXiv preprint arXiv:2010.11929* (2020)
- Ganin, Y., Ustinova, E., Ajakan, H., Germain, P., Larochelle, H., Laviolette, F., March, M., Lempitsky, V.: Domain-adversarial training of neural networks. *Journal of machine learning research* **17**(59), 1–35 (2016)
- Gao, I., Sagawa, S., Koh, P.W., Hashimoto, T., Liang, P.: Out-of-domain robustness via targeted augmentations. In: *International Conference on Machine Learning*. pp. 10800–10834. PMLR (2023)
- Gulrajani, I., Lopez-Paz, D.: In search of lost domain generalization. In: *International Conference on Learning Representations* (2021)
- He, K., Zhang, X., Ren, S., Sun, J.: Deep residual learning for image recognition. In: *Proceedings of the IEEE conference on computer vision and pattern recognition*. pp. 770–778 (2016)
- He, X., Hu, J., Lin, Q., Luo, C., Xie, W., Song, S., Khan, M.H., Shen, L.: Towards combating frequency simplicity-biased learning for domain generalization. *Advances in Neural Information Processing Systems* **37**, 31078–31102 (2024)

12. Hendrycks, D., Basart, S., Mu, N., Kadavath, S., Wang, F., Dorundo, E., Desai, R., Zhu, T., Parajuli, S., Guo, M., et al.: The many faces of robustness: A critical analysis of out-of-distribution generalization. In: Proceedings of the IEEE/CVF international conference on computer vision. pp. 8340–8349 (2021)
13. Henry, L.: Galaxy10 decals dataset. (2021)
14. Huang, G., Liu, Z., Van Der Maaten, L., Weinberger, K.Q.: Densely connected convolutional networks. In: Proceedings of the IEEE conference on computer vision and pattern recognition. pp. 4700–4708 (2017)
15. Ilse, M., Tomczak, J.M., Forré, P.: Selecting data augmentation for simulating interventions. In: International conference on machine learning. pp. 4555–4562. PMLR (2021)
16. Joly, A., Goëau, H., Kahl, S., Picek, L., Lorieul, T., Cole, E., Deneu, B., Serva-jean, M., Durso, A., Glotin, H., et al.: Overview of lifeclef 2022: an evaluation of machine-learning based species identification and species distribution prediction. In: International Conference of the Cross-Language Evaluation Forum for European Languages. pp. 257–285. Springer (2022)
17. Koh, P.W., Sagawa, S., Marklund, H., Xie, S.M., Zhang, M., Balsubramani, A., Hu, W., Yasunaga, M., Phillips, R.L., Gao, I., et al.: Wilds: A benchmark of in-the-wild distribution shifts. In: International conference on machine learning. pp. 5637–5664. PMLR (2021)
18. Kumar, A., Raghunathan, A., Jones, R., Ma, T., Liang, P.: Fine-tuning can distort pretrained features and underperform out-of-distribution. In: International Conference on Learning Representations (2022)
19. Li, D., Yang, Y., Song, Y.Z., Hospedales, T.M.: Deeper, broader and artier domain generalization. In: Proceedings of the IEEE international conference on computer vision. pp. 5542–5550 (2017)
20. Liu, Z., Mao, H., Wu, C.Y., Feichtenhofer, C., Darrell, T., Xie, S.: A convnet for the 2020s. In: Proceedings of the IEEE/CVF conference on computer vision and pattern recognition. pp. 11976–11986 (2022)
21. Long, M., Cao, Z., Wang, J., Jordan, M.I.: Conditional adversarial domain adaptation. *Advances in neural information processing systems* **31** (2018)
22. Park, D.S., Chan, W., Zhang, Y., Chiu, C.C., Zoph, B., Cubuk, E.D., Le, Q.V.: SpecAugment: A simple data augmentation method for automatic speech recognition. *arXiv preprint arXiv:1904.08779* (2019)
23. Pinson, H., Lenaerts, J., Ginis, V.: Linear cnns discover the statistical structure of the dataset using only the most dominant frequencies. In: International Conference on Machine Learning. pp. 27876–27906. PMLR (2023)
24. Qu, H., Xie, S.M.: Connect later: improving fine-tuning for robustness with targeted augmentations. In: Proceedings of the 41st International Conference on Machine Learning. pp. 41769–41786 (2024)
25. Sagawa, S., Koh, P.W., Lee, T., Gao, I., Xie, S.M., Shen, K., Kumar, A., Hu, W., Yasunaga, M., Marklund, H., et al.: Extending the wilds benchmark for unsupervised adaptation. In: International Conference on Learning Representations (2022)
26. Sainburg, T., Zorea, A.: Noisereduce: Domain general noise reduction for time series signals. *arXiv preprint arXiv:2412.17851* (2024)
27. Sarkar, A., Palit, S., Bhattacharya, U.: Demystifying galaxy classification: An elegant and powerful hybrid approach. In: 2024 39th International Conference on Image and Vision Computing New Zealand (IVCNZ). pp. 1–6. IEEE (2024)

28. Shen, K., Jones, R.M., Kumar, A., Xie, S.M., HaoChen, J.Z., Ma, T., Liang, P.: Connect, not collapse: Explaining contrastive learning for unsupervised domain adaptation. In: International conference on machine learning. pp. 19847–19878. PMLR (2022)
29. Su, J., Yu, X., Wang, X., Wang, Z., Chao, G.: Enhanced transfer learning with data augmentation. *Engineering Applications of Artificial Intelligence* **129**, 107602 (2024)
30. Sun, B., Feng, J., Saenko, K.: Correlation alignment for unsupervised domain adaptation. *Domain adaptation in computer vision applications* pp. 153–171 (2017)
31. Sun, B., Saenko, K.: Deep coral: Correlation alignment for deep domain adaptation. In: Computer vision–ECCV 2016 workshops: Amsterdam, the Netherlands, October 8-10 and 15-16, 2016, proceedings, part III 14. pp. 443–450. Springer (2016)
32. Tan, M., Le, Q.: Efficientnet: Rethinking model scaling for convolutional neural networks. In: International conference on machine learning. pp. 6105–6114. PMLR (2019)
33. Tellez, D., Balkenhol, M., Otte-Höller, I., Van De Loo, R., Vogels, R., Bult, P., Wauters, C., Vreuls, W., Mol, S., Karssemeijer, N., et al.: Whole-slide mitosis detection in h&e breast histology using phh3 as a reference to train distilled stain-invariant convolutional networks. *IEEE transactions on medical imaging* **37**(9), 2126–2136 (2018)
34. Venkateswara, H., Eusebio, J., Chakraborty, S., Panchanathan, S.: Deep hashing network for unsupervised domain adaptation. In: Proceedings of the IEEE conference on computer vision and pattern recognition. pp. 5018–5027 (2017)
35. Wang, G.: Galaxy morphology classification with densenet. In: *Journal of Physics: Conference Series*. vol. 2580, p. 012064. IOP Publishing (2023)
36. Wang, R., Wang, H., Luo, Q.: Galaxalign: Mimicking citizen scientists’ multimodal guidance for galaxy morphology analysis. In: Proceedings of the 33rd ACM International Conference on Multimedia. pp. 8636–8644 (2025)
37. Wang, S., Veldhuis, R., Brune, C., Strisciuglio, N.: What do neural networks learn in image classification? a frequency shortcut perspective. In: Proceedings of the IEEE/CVF International Conference on Computer Vision. pp. 1433–1442 (2023)
38. Wiles, O., Goyal, S., Stimberg, F., Rebuffi, S.A., Ktena, I., Dvijotham, K.D., Cemgil, A.T.: A fine-grained analysis on distribution shift. In: International Conference on Learning Representations (2021)
39. Wong, W.K., Lu, Y., Wu, J., Lai, Z., Li, X.: Approximate geometric structure transfer for cross-domain image classification. *Pattern Recognition* **159**, 111105 (2025)
40. Xu, C., Tian, X.: Semantic-aware mixup for domain generalization. In: 2023 International Joint Conference on Neural Networks (IJCNN). pp. 1–8. IEEE (2023)
41. Xu, Q., Zhang, R., Fan, Z., Wang, Y., Wu, Y.Y., Zhang, Y.: Fourier-based augmentation with applications to domain generalization. *Pattern Recognition* **139**, 109474 (2023)
42. Xu, Q., Zhang, R., Zhang, Y., Wang, Y., Tian, Q.: A fourier-based framework for domain generalization. In: Proceedings of the IEEE/CVF conference on computer vision and pattern recognition. pp. 14383–14392 (2021)
43. Yan, S., Song, H., Li, N., Zou, L., Ren, L.: Improve unsupervised domain adaptation with mixup training. arXiv preprint arXiv:2001.00677 (2020)
44. Yao, H., Wang, Y., Li, S., Zhang, L., Liang, W., Zou, J., Finn, C.: Improving out-of-distribution robustness via selective augmentation. In: International Conference on Machine Learning. pp. 25407–25437. PMLR (2022)

45. Yun, S., Han, D., Oh, S.J., Chun, S., Choe, J., Yoo, Y.: Cutmix: Regularization strategy to train strong classifiers with localizable features. In: Proceedings of the IEEE/CVF international conference on computer vision. pp. 6023–6032 (2019)
46. Zhang, H., Cisse, M., Dauphin, Y.N., Lopez-Paz, D.: mixup: Beyond empirical risk minimization. arXiv preprint arXiv:1710.09412 (2017)
47. Zhou, K., Yang, Y., Hospedales, T., Xiang, T.: Deep domain-adversarial image generation for domain generalisation. In: Proceedings of the AAAI conference on artificial intelligence. vol. 34, pp. 13025–13032 (2020)
48. Zhou, K., Yang, Y., Hospedales, T., Xiang, T.: Learning to generate novel domains for domain generalization. In: European conference on computer vision. pp. 561–578. Springer (2020)